Geophys. J. Int. (1995) **123**, 1–15

Seismic attenuation values obtained from instantaneous-frequency matching and spectral ratios

Michael P. Matheney and Robert L. Nowack
Department of Earth and Atmospheric Sciences, Purdue University, West Lafayette, IN 47907, *USA*

Accepted 1994 December 2. Received 1994 March 11

SUMMARY

In this paper, attenuation values are obtained from seismic data using instantaneous-frequency matching and spectral ratios. To obtain differential t^* values using instantaneous-frequency matching, a near offset reference pulse is attenuated until the resulting instantaneous frequency matches the observed value at the receiver. Prior to matching, filtering can be applied to each trace in order to reduce the effects of noise on the calculated instantaneous frequencies. In the second method, the spectral ratio between a receiver pulse and a reference pulse is used to obtain differential t^* values. To obtain an unbiased estimate, a variable spectral bandwidth is used depending on the noise level of the data. The two methods are tested using synthetic traces and then applied to crustal refraction data from the 1986 PASSCAL Ouachita experiment. Results show that the differential t^* values obtained using filtered, instantaneous-frequency matching are consistent with and have less scatter than those obtained from spectral ratios with a variable bandwidth.

Key words: instantaneous frequency, seismic attenuation, spectral ratios.

INTRODUCTION

Both the elastic and anelastic properties of a medium are required to describe the propagation of seismic waves in the Earth. The elastic characteristics of the subsurface can be inferred from observed traveltimes of seismic body waves, as well as from phase velocities of seismic surface waves. Anelastic subsurface properties can be estimated from seismic amplitude decay (Brzostowski & McMechan 1992; Braile 1977), rise times (Gladwin & Stacey 1974), pulse broadening (Wright & Hoy 1981), spectral ratios (Bath 1974), analytical signal methods (Taner, Koehler & Sheriff 1979), and wavelet modelling (Jannsen, Voss & Theilen 1985). Comparisons of different techniques by Tonn (1989, 1991), Badri & Mooney (1987), Tarif & Bourbie (1987), and Jannsen *et al.* (1985) conclude that each of the methods for determining anelastic attenuation have situations in which they perform well. Pulse-broadening and rise-time techniques work well when only a small part of the signal is available for analysis, but are often source-pulse-dependent (Blair & Spaths 1984). Amplitude-decay techniques are sensitive to focusing and defocusing effects from the seismic velocity structure. The techniques based on instantaneous frequency and spectral ratios are less sensitive to focusing effects (Tonn 1991; Badri & Mooney 1987; Carpenter & Sanford 1985), and are used for the basis of this study.

In the first technique investigated in this study, the instantaneous frequency is computed and then matched between an attenuated reference pulse and an observed pulse to determine the differential attenuation. In the second technique, a variable-bandwidth spectral ratio between a reference and observed pulse is used to determine the attenuation values. Both methods are tested using synthetic data and then applied to crustal refraction data from the 1986 PASSCAL Ouachita experiment.

SEISMIC ATTENUATION FROM INSTANTANEOUS-FREQUENCY MATCHING

Complex seismic trace analysis

Complex trace analysis can be used to obtain the signal envelope and the instantaneous frequency, a time-varying measure of frequency. The concept of instantaneous frequency was described by Gabor (1946). Geophysical applications of instantaneous frequency include those of Taner *et al.* (1979), Tonn (1989, 1991) and Barnes (1991, 1993). Taner *et al.* (1979) used instantaneous frequency directly to aid in the interpretation of seismic sections. Tonn (1989, 1991) and Barnes (1991) obtained relations between instantaneous frequency and seismic attenuation.

Using complex trace analysis, a given seismic trace $y(t)$ can be represented by its envelope $a(t)$ and phase $\theta(t)$. The real trace can be written

$$y(t) = a(t)\cos\theta(t), \tag{1}$$

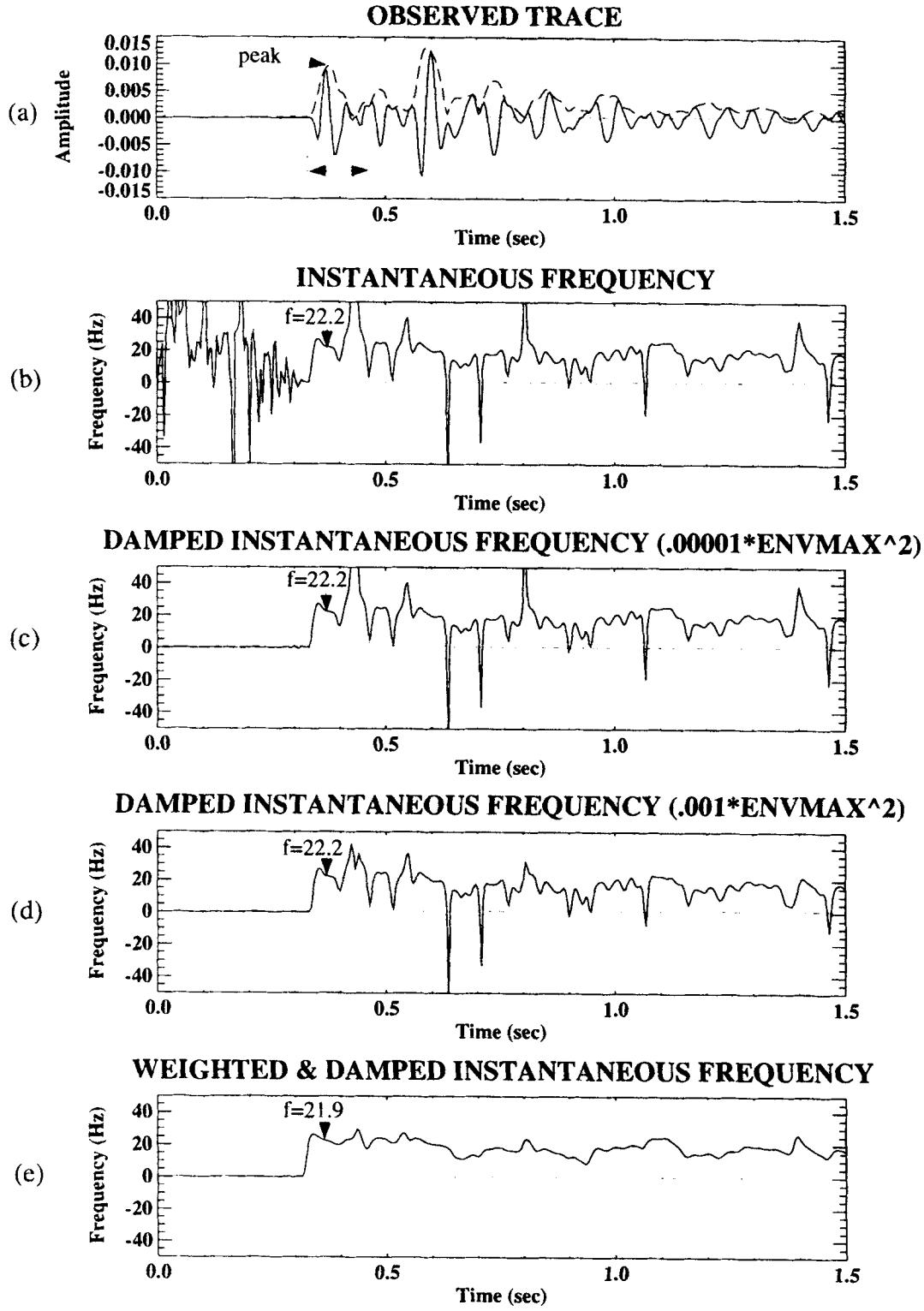

Figure 1. (a) Seismic trace showing envelope amplitude and length of window used to isolate a reference pulse. (b) Instantaneous frequency along the trace. (c) Damped instantaneous frequency with a damping of 0.00001 times the envelope maximum squared. (d) Damped instantaneous frequency with a damping of 0.001 times the envelope maximum squared. (e) Damped and weighted instantaneous frequency using a nine point, amplitude squared weighting and a damping of 0.001.

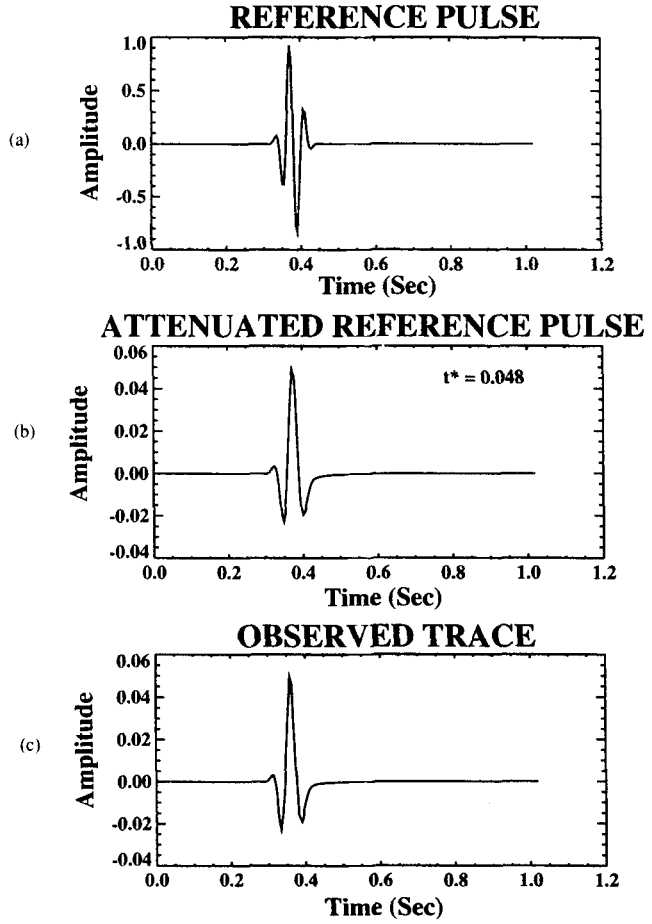

Figure 2. Synthetic example of instantaneous-frequency matching. (a) Unattenuated reference pulse. (b) The reference pulse attenuated with a t^* value equal to 0.048 such that the instantaneous frequency matches that of the observed pulse. (c) The observed trace to which the instantaneous frequency of the attenuated reference pulse is matched.

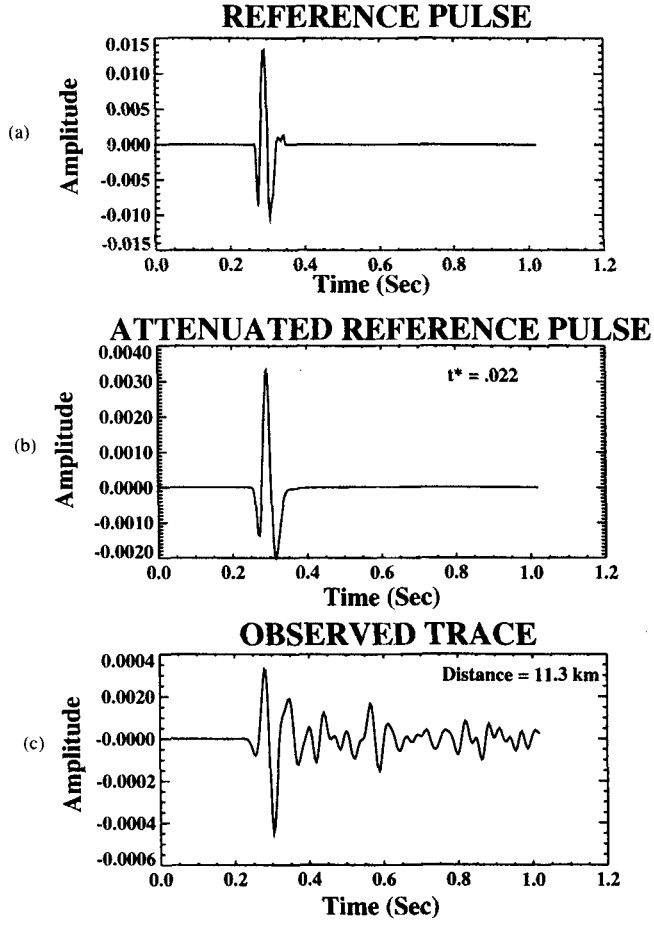

Figure 3. Real data example of instantaneous-frequency matching. (a) Windowed near-offset reference pulse. (b) The reference pulse which is attenuated with a t^* value equal to 0.022. (c) The observed trace whose *P*-wave arrival is being matched.

and the quadrature trace as

$$y^*(t) = a(t)\sin\theta(t). \tag{2}$$

The complex trace $z(t)$ is then given by (Taner *et al.* 1979)

$$z(t) = y(t) + iy^*(t) = a(t)e^{i\theta(t)}. \tag{3}$$

The Hilbert transform is used to obtain the quadrature trace. Once the real and quadrature traces are found, the instantaneous amplitude and phase are derived from

$$a(t) = [y(t)^2 + y^*(t)^2]^{1/2} \tag{4}$$

and

$$\theta(t) = \tan^{-1}\left[\frac{y^*(t)}{y(t)}\right]. \tag{5}$$

The instantaneous frequency, $f(t)$, is the rate of change of the instantaneous phase:

$$f(t) = \frac{1}{2\pi}\frac{d}{dt}(\theta(t)) \tag{6}$$

(Barnes 1991). Taking the derivative of the instantaneous phase results in

$$f(t) = \left(\frac{1}{2\pi}\right)\frac{y(t)\dfrac{dy^*(t)}{dt} - y^*(t)\dfrac{dy(t)}{dt}}{y^2(t) + y^{*2}(t)}. \tag{7}$$

Unlike a Fourier frequency, the instantaneous frequency can have large-amplitude positive and negative spikes. Fig. 1 illustrates these phenomena with an observed seismic trace. Fig. 1(a) shows the seismic trace and its envelope, and Fig. 1(b) shows the instantaneous frequency. Large spikes in the instantaneous frequency occur when the denominator of eq. (7), which is equal to the squared amplitude, approaches zero more rapidly than the numerator. In this study, the large spikes are not of interest and can be reduced by adding a small damping factor. This results in

$$f(t) = \left(\frac{1}{2\pi}\right)\frac{y(t)\dfrac{dy^*(t)}{dt} - y^*(t)\dfrac{dy(t)}{dt}}{a^2(t) + \varepsilon^2}. \tag{8}$$

Figs 1(c) and (d) show the damped instantaneous frequency, with ε^2 values of 0.00001 and 0.001 times the maximum envelope squared used for the damping. In both cases, the spiky appearance of the instantaneous frequency in low-

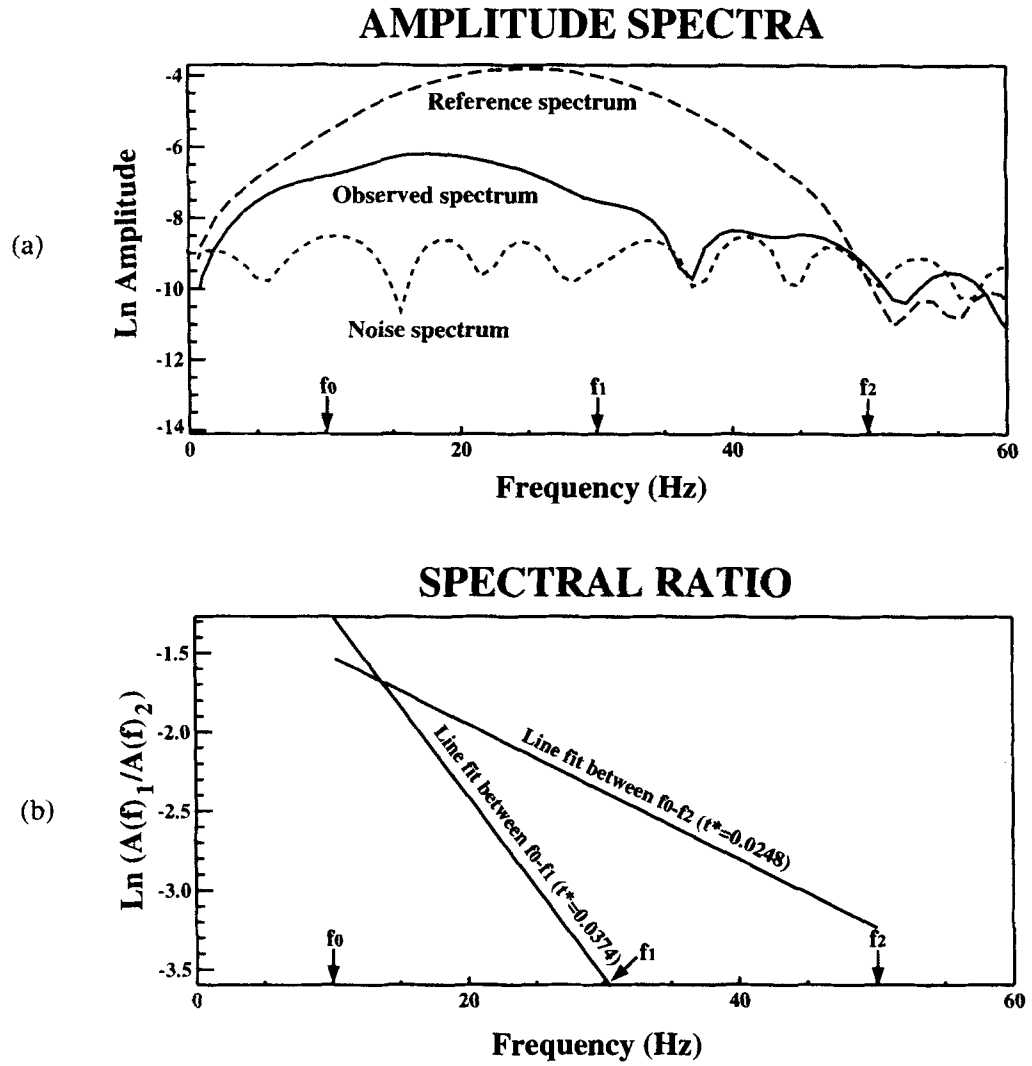

Figure 4. (a) Amplitude spectra representing a reference pulse, an observed pulse and the background noise level. Note that the observed pulse's spectrum flattens out at the noise level of the trace. (b) Corresponding line fits for a spectral ratio with a bandwidth between f_0 and f_1 and a bandwidth between f_0 and f_2. If the bandwidth is selected too wide, the resulting line fit will have a slope that is less than the actual value.

envelope-amplitude areas, such as before the first arrival, is eliminated and subsequent spikes within the trace are reduced. The damping does not significantly affect the instantaneous-frequency value where the envelope amplitude is large.

In addition to damping, the instantaneous-frequency values can also be weighted. This results in

$$f(t)=\frac{\int_{t-T}^{t+T} f(t')W(t')\,dt'}{\int_{t-T}^{t+T} W(t')\,dt'}, \tag{9}$$

where in this study the weighting, $W(t)$, is taken to be the squared envelope amplitude. For this choice of $W(t)$, the weighted instantaneous frequency approaches the average Fourier spectral frequency as T becomes large (Barnes 1993; Saha 1987). The weighting is also necessary to stabilize the calculated instantaneous frequency further. In Fig. 1(e), a nine point, or 0.036 s, window for the instantaneous-frequency weighting is used. This value was found to be sufficient for stabilizing the values while leaving the necessary detail in the instantaneous frequency, and is used for subsequent instantaneous-frequency weightings.

In Figs 1(b)–(e), a particular value of the damped and weighted instantaneous frequency is shown by an arrow at the point where the envelope reaches its first maximum after the arrival time. The first envelope peak is chosen as the point at which to evaluate the instantaneous frequency because of its relative stability. Note from Figs 1(b)–(e) that the damping and weighting used have only a small effect on the instantaneous frequency at the first-arrival envelope peak. This value, however, will not necessarily be a stationary point with time for the instantaneous frequency along the pulse.

Localization of the pulse in the time-domain

The time-domain isolation of a reference pulse is needed for both instantaneous-frequency matching and spectral ratios. The localization of a reference pulse is accomplished by

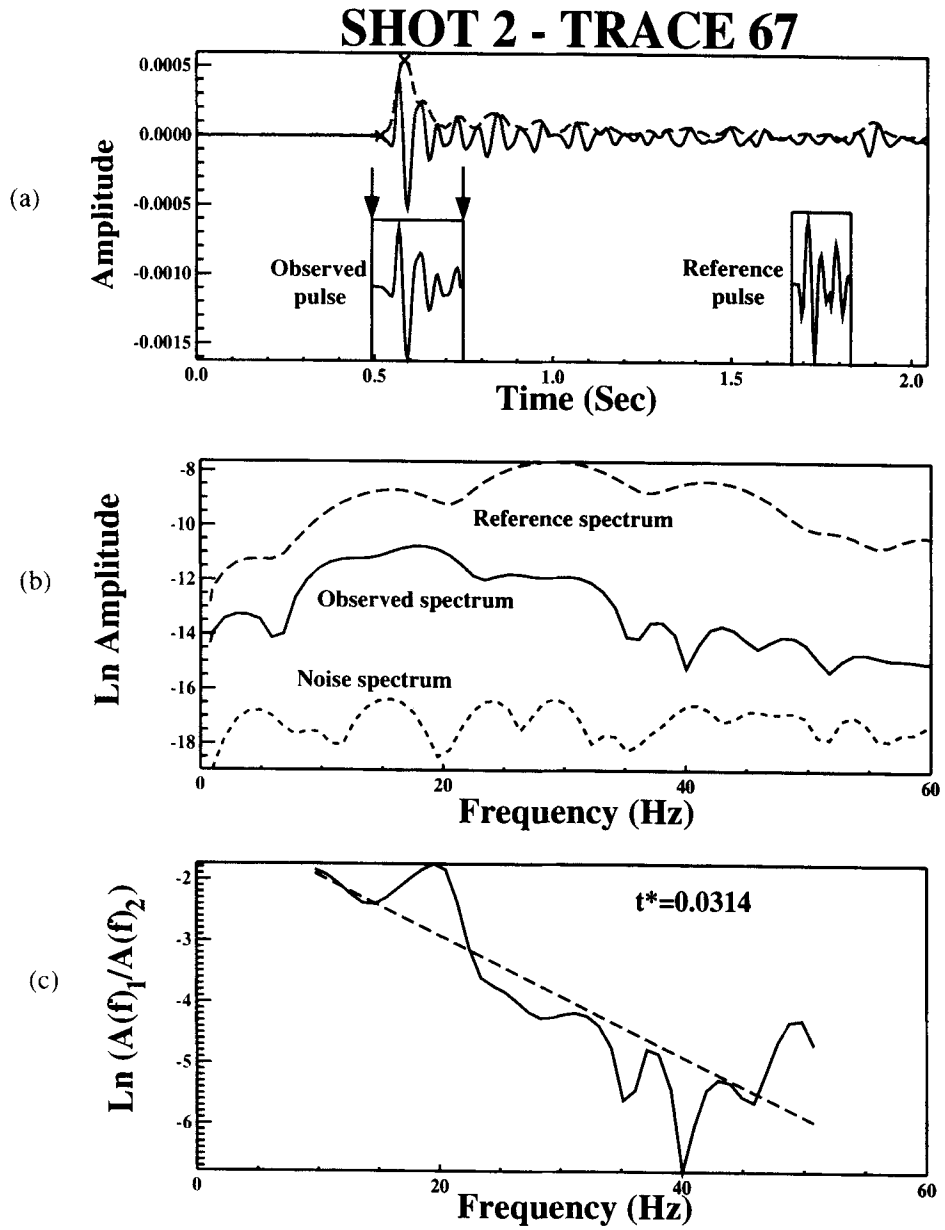

Figure 5. Example of the spectral ratio method used on a trace with a high signal-to-noise ratio. (a) Seismic trace with windowed *P* wave, also showing the reference pulse. (b) Amplitude spectra for the reference pulse, the observed pulse and the noise. (c) Corresponding line fit with a bandwidth of 10–50 Hz. Note that the high-frequency cut-off can extend up to 50 Hz.

multiplying the trace by a cosine bell window function, $H(t)$, about the pulse of interest. In the analysis here, the start of the pulse is obtained by interactively picking the pulse's arrival time. The end of the pulse is selected by taking the time difference between the start of the pulse and the first envelope peak, and then multiplying by three. The beginning of the window is chosen to be slightly earlier than the arrival time, by 5 per cent of the total window length. This is done to prevent the cosine bell window from changing the pulse shape. As an example, in Fig. 1(a) the arrows beneath the *P* wave are used to show the length of the window. All windowing uses a 5 per cent cosine taper at each end of the window to extract the first-arrival pulse, $p(t) = H(t)y(t)$. The cosine bell window minimizes any discontinuities between the beginning and end of the windowed pulse, while having a minimal effect on the shape of the pulse.

Matching of instantaneous frequencies

The windowing procedure described above is first used to extract a near-offset reference pulse, $p_r(t)$. The windowed reference pulse is then zero-padded to 256 points and the Fourier transform is taken, resulting in $P_r(\omega)$. For all derived equations, the Fourier transform notation is taken to be $y(t) = \int_{-\infty}^{\infty} Y(\omega) e^{-i\omega t} (d\omega/2\pi)$. The damped and weighted instantaneous frequency of the arrival at the peak of the envelope is determined for every trace in the shot gather. A damping value ε^2 of 0.001 times the squared peak envelope

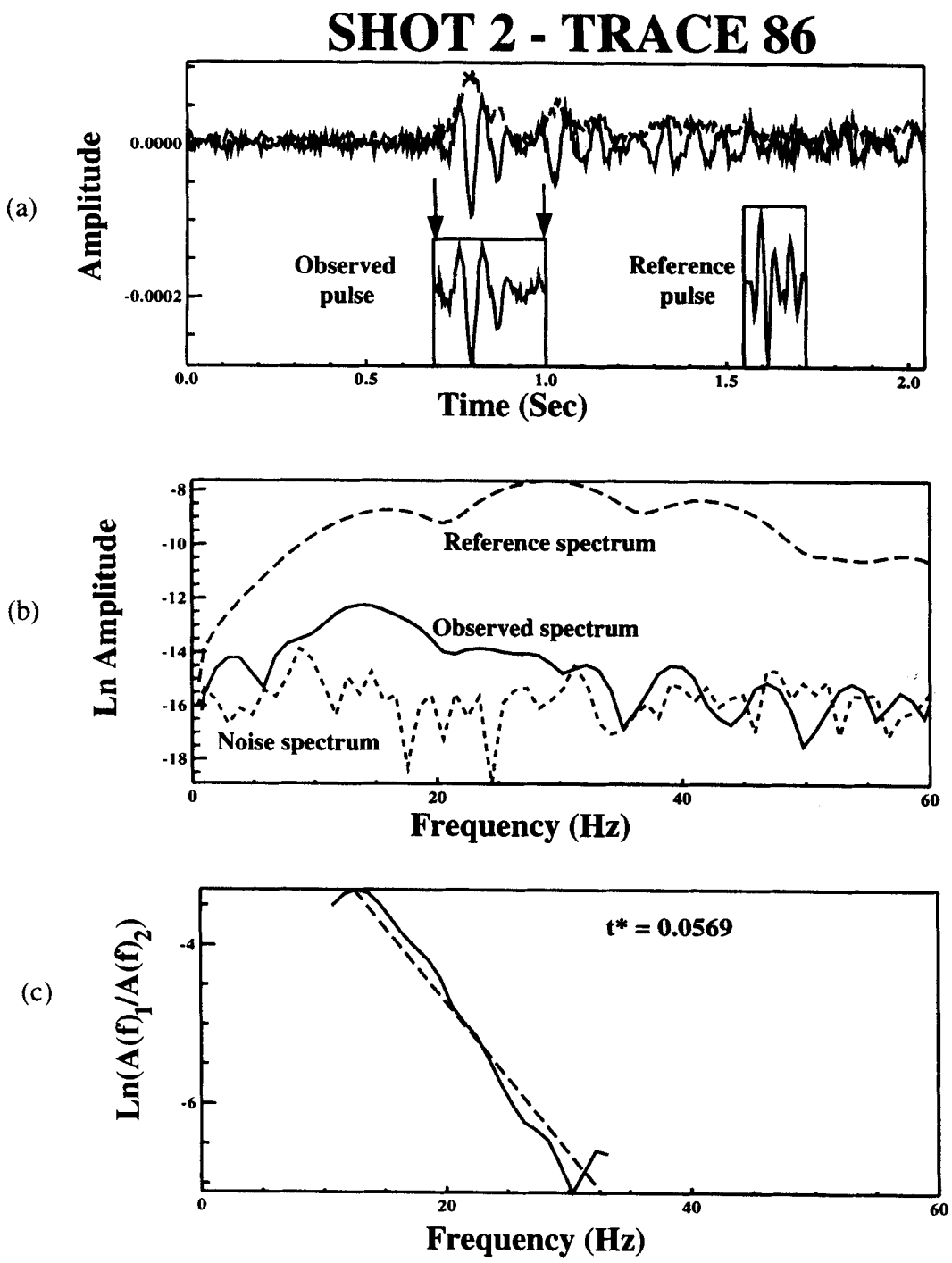

Figure 6. Example of the spectral-ratio method used on a trace with a low signal-to-noise ratio. (a) Seismic trace with windowed *P* wave, also showing the reference pulse. (b) Amplitude spectra for the reference pulse, the observed pulse and the noise. (c) Corresponding line fit with a bandwidth of 10–33 Hz. Note that the high-frequency cut-off has to be reduced from 50 to 33 Hz.

amplitude along with a nine point weighting is used. The reference pulse is then attenuated using a causal attenuation operator. The attenuated reference pulse is given by

$$p_r^{att}(t) = \mathrm{IFFT}[P_r(\omega)A(\omega)], \tag{10}$$

where IFFT refers to the inverse fast Fourier transform, and

$$A(\omega) = \exp\left[-\frac{i\omega}{\pi}t^* \ln\left(\frac{\omega}{\omega_r}\right)\right]\exp\left(-\frac{\omega}{2}t^*\right), \tag{11}$$

where

$$t^* = \int \frac{Q^{-1}(s)}{c(s)}ds \tag{12}$$

is the causal attenuation operator (Aki & Richards 1980). In these equations, $c(s)$ is the velocity for the reference radial frequency ω_r, Q is the seismic quality factor, and s is the length along the ray. For this study, a reference frequency of 25 Hz is

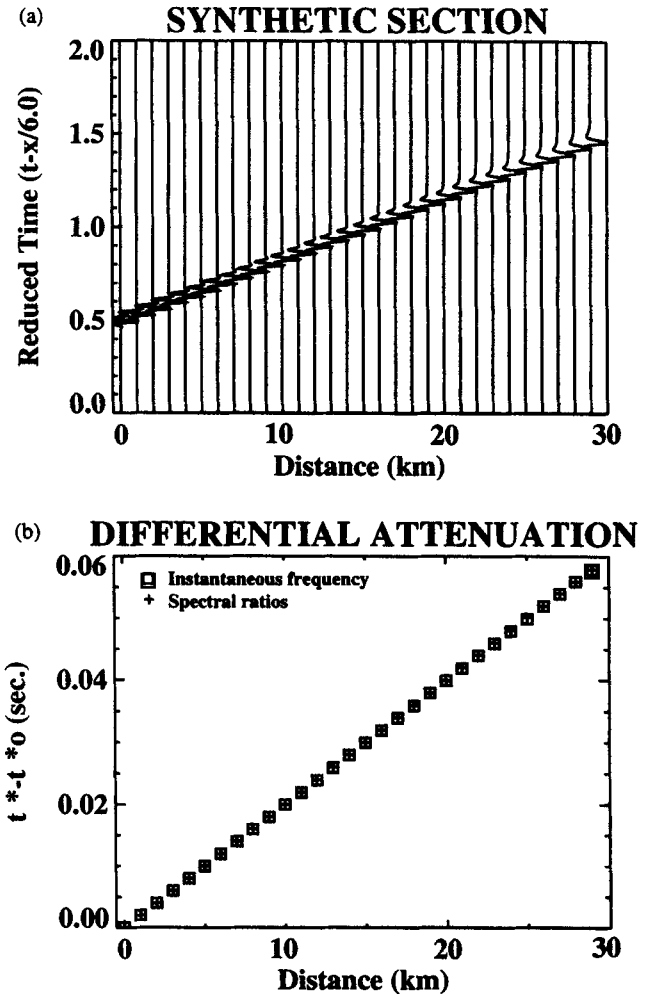

Figure 7. Synthetic noise-free example. (a) Synthetic section simulating a source wavelet of 25 Hz propagating through a medium with a Q of 100. (b) The resulting differential attenuation values obtained using the instantaneous-frequency and spectral-ratio methods.

used for the attenuation operator. The degree of attenuation is controlled by the attenuation parameter, t^*. The attenuated reference spectrum is then inverse Fourier transformed to give $p_r^{att}(t)$, and the instantaneous frequency at the peak of the envelope is calculated.

The attenuation value, t^*, that matches the instantaneous frequency of the observed pulse with that of the attenuated reference pulse is obtained by iterating the linearized relation

$$(f^{obs} - f^{attref}) \cong \left.\frac{df}{dt^*}\right|_{t^*_{attref}} (t^* - t^*_{attref}), \tag{13}$$

where $f^{obs} - f^{attref}$ is the difference between the instantaneous frequency of the observed pulse and that of the attenuated reference pulse; df/dt^* is the change of instantaneous frequency of the reference pulse due to a change in t^*; t^*_{attref} is the previous attenuation value; and t^* is the updated attenuation value for attenuating the reference pulse. The derivative df/dt^* is approximated by a calculated finite difference. Rearranging eq. (13) gives the working equation

$$t^* \cong t^*_{attref} + \frac{f^{obs} - f^{attref}}{df/dt^*}. \tag{14}$$

This relation is applied iteratively until the difference between the observed and the calculated instantaneous frequencies of the attenuated reference pulse is less than 0.3 Hz. When a match in instantaneous frequency is achieved, the differential attenuation is obtained directly from the value of t^* used to attenuate the reference pulse. A similar matching procedure using pulse rise times is given by Blair & Spaths (1984).

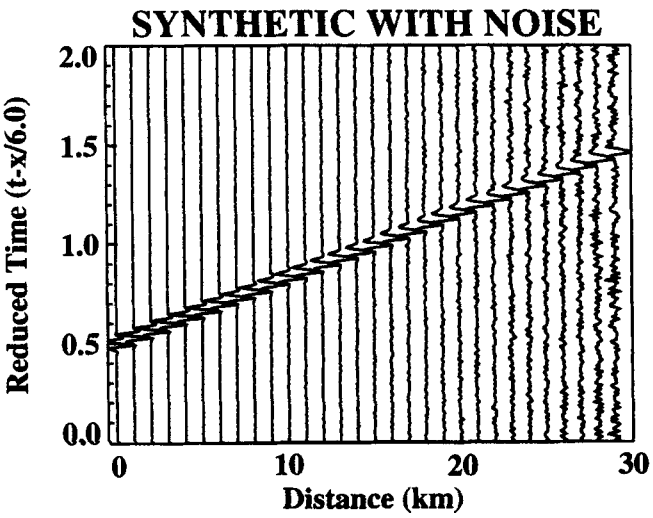

Figure 8. Representative noise synthetic seismic section with a 25 Hz source wavelet propagating through a medium with a Q of 100 with band-passed Gaussian noise added.

A synthetic example using a Gabor wavelet is used to test the algorithm. The Gabor wavelet model can be written

$$x(t) = \cos[2\pi f_0(t - t_0) + v] \exp[-4\pi^2 f_0^2 (t - t_0)^2/\gamma^2] \tag{15}$$

(Červený, Molotkov & Pšenčík 1977). In the example, the parameters $\gamma = 4.5$, $f_0 = 25$ Hz, and $v = 2\pi/5$ are used. In Fig. 2, a Gabor wavelet is attenuated with the constant-Q, causal attenuation operator given above, with $c = 5.0\,km\,s^{-1}$ and $Q = 50$. Fig. 2(a) shows the windowed, unattenuated reference pulse. Fig. 2(b) shows the reference pulse after it has been attenuated so that the instantaneous frequency at the peak envelope amplitude matches the observed pulse shown in Fig. 2(c) at a distance of 12.0 km. The correct value of attenuation, $t^* = 0.048$, is retrieved.

A corresponding real data example from the 1986 Ouachita PASSCAL experiment is shown in Fig. 3. The near-source, unattenuated reference pulse is shown in Fig. 3(a). This is attenuated in Fig. 3(b) until the instantaneous frequency matches that of the observed P wave at a distance of 11.3 km (Fig. 3c). A value of $t^* = 0.022$ is obtained for this case.

DIFFERENTIAL ATTENUATION OBTAINED FROM SPECTRAL RATIOS

Spectral ratios can also be used to obtain the differential attenuation between a reference pulse and other observed pulses of a shot gather. The ratio of the spectra between a reference pulse and each of the other pulses in the shot gather is taken over a selected frequency band. The general formula is

$$\frac{|A(\omega, \mathbf{x})|}{|A_r(\omega, \mathbf{x}_r)|} = \frac{|S(\omega)B(\theta_1)C_1(\omega, \theta_1)G(\omega, \mathbf{x})C_2(\omega, \theta_2)I(\omega)| \exp(-\omega t^*/2)}{|S(\omega)B_r(\theta_1^r)C_1(\omega, \theta_1^r)G_r(\omega, \mathbf{x}_r)C_2(\omega, \theta_2^r)I_r(\omega)| \exp(-\omega t_r^*/2)}, \tag{16}$$

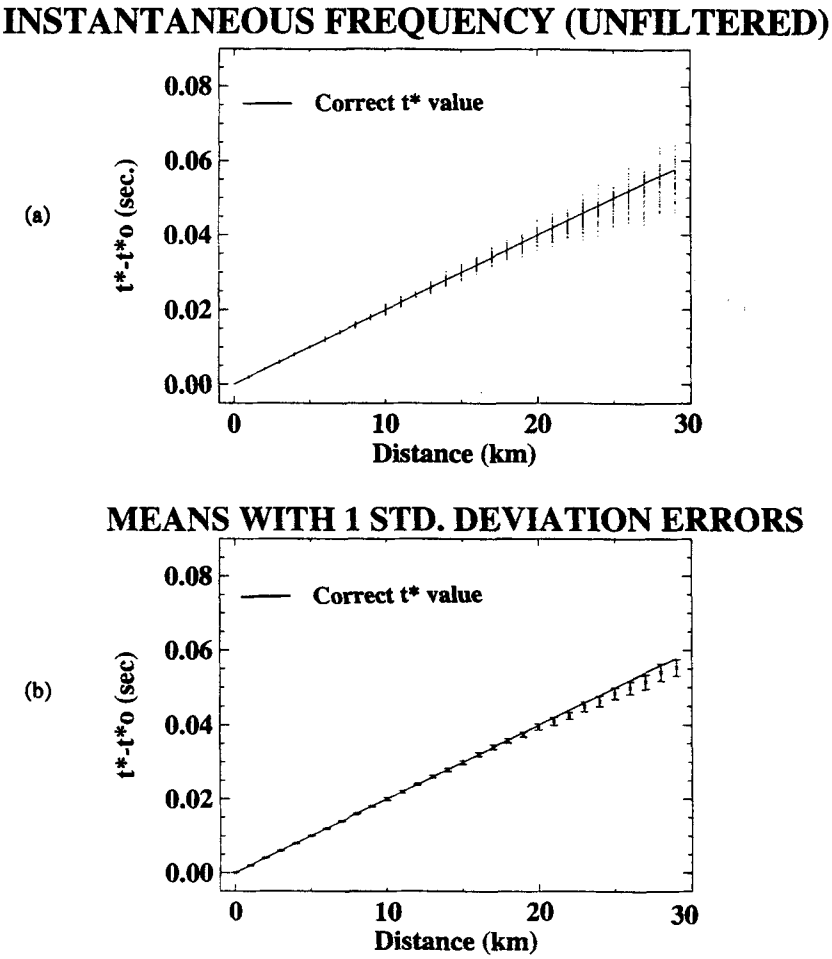

Figure 9. (a) Differential attenuation values obtained by applying the instantaneous-frequency matching (IFM) to 50 noisy seismic sections. (b) The calculated means with one standard deviation uncertainties. Note the bias in the calculated attenuation values as the signal-to-noise ratio decreases.

where $|A(\omega,\mathbf{x})|$ and $|A(\omega,\mathbf{x}_r)|$ are the amplitude spectra at receiver distances $\mathbf{x}$ and $\mathbf{x}_r$ from the source. $S(\omega)$ is the source spectrum, $B(\theta_1)$ is the source radiation pattern, $C_1(\omega,\theta_1)$ and $C_2(\omega,\theta_2)$ are the local source and receiver shallow crustal effects where θ_1 and θ_2 are the source and receiver ray angles, $G(\omega,\mathbf{x})$ is the path geometric spreading, and $I(\omega)$ is the instrument response. Finally, t^* is equal to $\int Q^{-1}ds/c$ where Q is the attenuation and c is the velocity along the ray. The subscript or superscript r refers to the reference pulse. For a common shot gather with an explosive source, and with the stations using the same type of instrument, $S(\omega)$, $B(\theta)$ and $I(\omega)$ cancel. In addition, by making the assumptions that the local source and receiver effects $C_1(\omega)$ and $C_2(\omega)$ approximately cancel between the reference and other pulses, and that the geometrical spreading $G(\omega,\mathbf{x})$ is independent of frequency, then eq. (16) takes the form (Bath 1974)

$$\ln\frac{|A(\omega)|}{|A_r(\omega)|}=\ln\frac{|G|}{|G_r|}-\frac{\omega}{2}(t^*-t_r^*). \tag{17}$$

This is the equation of a line with slope $-(t^*-t_r^*)/2$ with radial frequency. By fitting a least-squares line through the line of this spectral ratio, the differential attenuation $(t^*-t_r^*)$ is obtained from the slope of the line with frequency.

The window length and spectral bandwidth are two variables that can affect the calculated attenuation values derived from the spectral ratios. First, by using a short time window, secondary arrivals can be removed. This in turn removes spectral holes that result from interfering pulses, which can cause problems when performing a line fit to the spectral ratio. However, too short a time window can cause the spectral ratios to become highly variable (Sams & Goldberg 1990; Ingram *et al.* 1985), and also cause a poor sampling of the lower frequencies. For this study, the same cosine bell window as described in the instantaneous-frequency matching section is used to isolate the pulses for the spectral ratios. The variable window length of three times the first-arrival time to envelope peak effectively isolates the first arrival and is not so short that the spectral ratios become unstable.

The determination of a bandwidth is also a problem that can greatly influence the calculated differential attenuation values. Previous work, including that of Badri & Mooney (1987) and Carpenter & Sanford (1985), used a fixed bandwidth for all spectral ratios. When using a fixed bandwidth, part of the usable spectrum may not be included for the near-source traces. For the far-offset traces, however, the bandwidth may be too large. None the less, use of the largest bandwidth that

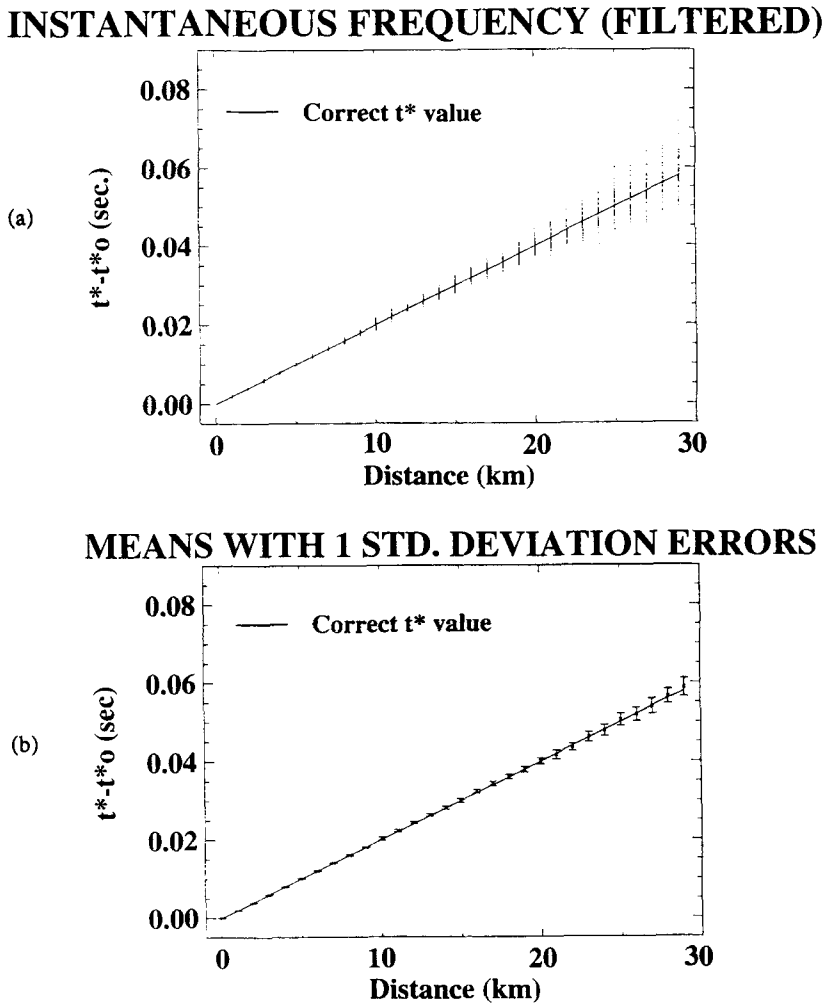

Figure 10. (a) Differential attenuation values obtained by applying the filtered instantaneous-frequency matching method (IFM/F) to 50 noisy sections. (b) The calculated means with one standard deviation uncertainties. Note that the bias in the differential attenuation values has been removed by using a noise-dependent variable low-pass filter.

the data will allow stabilizes the calculated attenuation values. This is a result of the larger number of points used for the least-squares line fit, which minimizes the effects spectral holes have on the line fit. Even though a large bandwidth is desired (White 1992), the possibility of running off the usable spectrum and into the background noise is increased.

Fig. 4 illustrates the problem of selecting a bandwidth for a spectral ratio. In this example, the spectrum for the observed pulse flattens out for frequencies greater than 35 Hz. This is due to the background noise level of the trace, which is shown by the noise spectrum. If the spectral ratio extends higher than the point where the noise level dominates, an incorrect attenuation value will be obtained. This is illustrated in Fig. 4(b), where the bandwidth for the spectral ratio is between f_0 and f_2. In this case, the bandwidth is too wide, and the calculated slope of the least-squares line fit is lower than the correct value. By decreasing the bandwidth from frequency f_2 down to frequency f_1, the part of the spectral ratio between f_1 and f_2 that is flat due to the background noise level is eliminated, and the least-squares slope is increased, giving the correct t^* value. Use of a reduced spectral bandwidth about the peak of the pulse's amplitude spectrum could eliminate this bias, but would also restrict the frequency bandwidth. This can cause instability in the calculated attenuation values if any spectral holes are present in either the reference spectrum or the observed pulse's spectrum.

A reasonable approach is to determine the largest usable bandwidth from the instrument response and noise level of the trace. First, a maximum bandwidth is selected based on the instrument response and the frequency of the reference pulse. This study uses a maximum bandwidth from 10 to 50 Hz. As the distance from the shot to the receiver increases, the high-frequency cut-off for the spectral ratio is lowered, based on the point where the pulse spectrum is reduced to the noise level. This determines the variable bandwidth for the spectral ratio.

As an example, Fig. 5(a) shows an observed trace from the 1986 PASSCAL Ouachita experiment with a high signal-to-noise ratio, the windowed *P*-wave arrival, and the reference pulse. In Fig. 5(b) the spectra of the reference and observed pulses, along with the noise spectrum, are shown. The noise level is determined by removing a portion of the trace before the first arrival. In this case, the full bandwidth from 10 to 50 Hz is used for the spectral ratio shown in Fig. 5(c), since the noise level is low relative to the observed pulse.

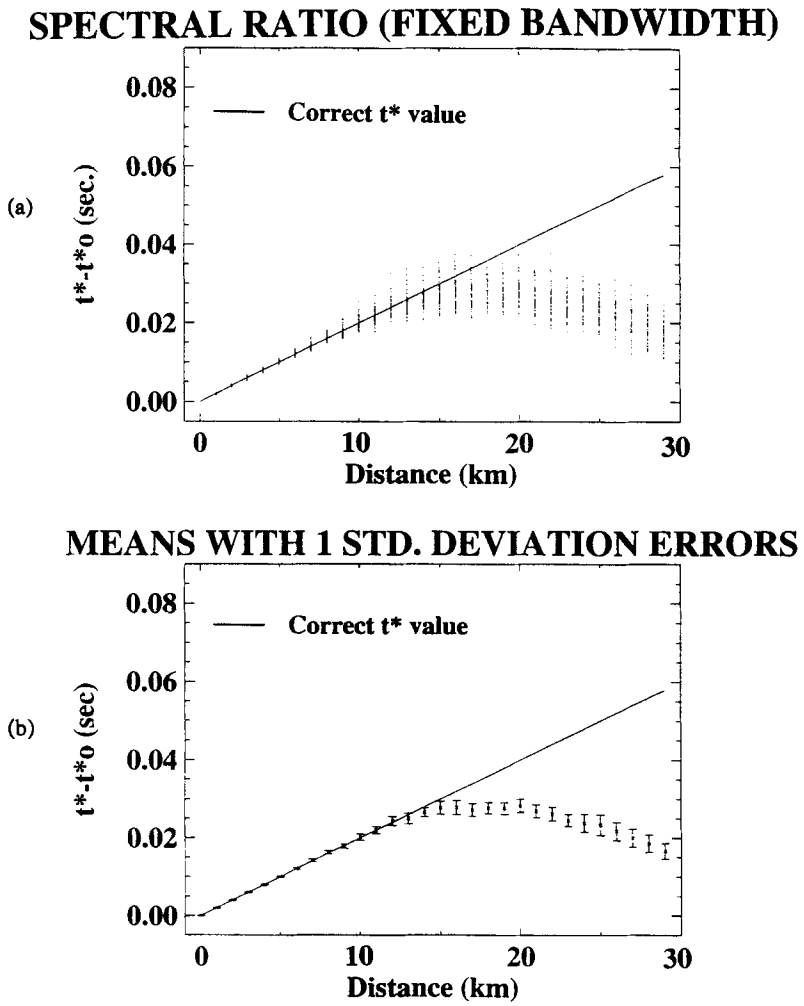

Figure 11. (a) Differential attenuation values obtained by applying the fixed-bandwidth spectral-ratio method (SR/FB) to 50 noisy seismic sections. (b) The calculated means with an uncertainty of one standard deviation. Note the bias in the attenuation values as the decreasing signal-to-noise ratio away from the shot location flattens the spectral ratio.

In Fig. 6(a), a trace with a lower signal-to-noise ratio is shown along with the windowed P wave and the reference pulse. The noise level for this trace, shown in Fig. 6(b), causes the observed pulse's spectrum to flatten at the noise level (approximately 35 Hz). If the spectral ratio were performed out to 50 Hz, the least-squares slope would be decreased by almost one-half, and the resulting t^* estimate would be in error. Therefore, the upper frequency cut-off is lowered to 33 Hz, or the point where the observed spectrum decreases to the noise level shown in Figs 6(b) and (c).

SYNTHETIC COMPARISON OF THE METHODS

The instantaneous-frequency and spectral-ratio methods described above are first applied to synthetic traces. The most prevalent problem when calculating attenuation values is the effect of noise on the estimates. Noise in this case includes both random background noise and interference from secondary arrivals. Interfering arrivals can cause the largest uncertainties in the calculated attenuation values.

The synthetic seismographs are generated using the Gabor wavelet model and constant-Q attenuation operator described above. Fig. 7(a) shows a noise-free synthetic seismic section created using an initial Gabor pulse with a frequency of 25 Hz, $\gamma = 4.5$ and $\nu = 2\pi/5$, and propagated through a half-space model with a velocity of 5.0 km s^{-1} with a Q of 100. The results of applying both the instantaneous-frequency and spectral-ratio methods are shown in Fig. 7(b). The correct attenuation values are obtained using both methods for all distances.

In the second synthetic test, 50 noisy synthetic seismogram sections are generated with the same 25 Hz wavelet, as shown in the first example, and propagated through a medium with a Q of 100. Gaussian noise is generated using the random number routines in Press *et al.* (1992). The Gaussian random noise is then low-pass filtered with a five pole Butterworth filter with a cut-off frequency of 60 Hz, and added to the synthetic traces. A representative noisy section is shown in Fig. 8. Note that the traces are unit-normalized and the noise level is the same for each of the traces. The apparent increase in noise level with distance results from the amplitude decay of the main pulse.

First, instantaneous-frequency matching with no filtering is applied to an ensemble of 50 noisy seismic sections. As the

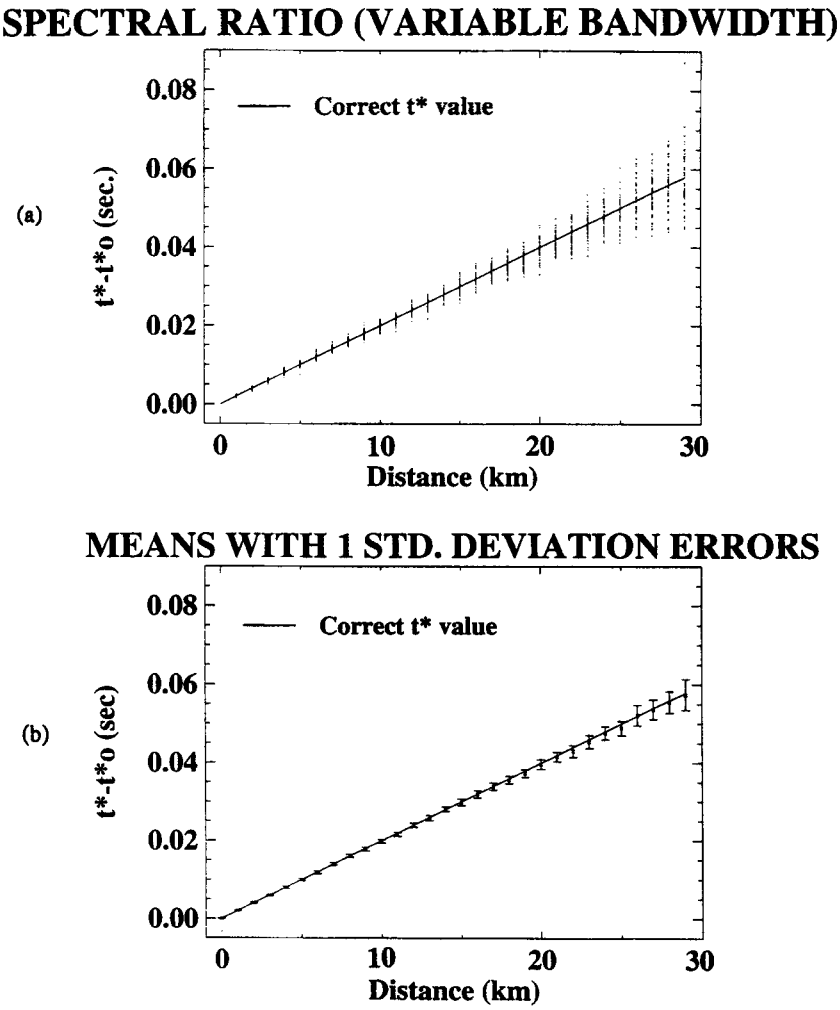

Figure 12. (a) Differential attenuation values obtained by applying the variable-bandwidth spectral-ratio method (SR/VB) to 50 noisy seismic sections. (b) The calculated means with an uncertainty of one standard deviation. Note that the bias in the attenuation values is removed by lowering the cut-off frequency for the spectral ratio as the noise level is increased.

signal-to-noise ratio decreases with increasing distance, a bias is introduced in the calculated attenuation values. Fig. 9(a) shows the resulting estimates of the attenuation for the 50 noisy record sections, where each small dot is an attenuation estimate. Fig. 9(b) shows the mean and standard deviation for the 50 realizations at each distance. The mean differential attenuation values are lower than the correct values for the same reason that spectral-ratio estimates are lowered if the bandwidth is too wide. The instantaneous-frequency estimates are being increased due to the noise, and this in turn lowers the calculated differential attenuation. Unlike spectral ratios, where this bias can be removed by limiting the bandwidth for the spectral ratio, the traces need to be low-pass filtered to remove as much noise as possible before calculating the instantaneous frequency. The procedure involves determining the frequency where the pulse amplitude spectrum is at the level of the noise amplitude spectrum (Fig. 4). This is accomplished by using a portion of the trace prior to the first arrival and calculating the noise amplitude spectrum. The point determined using this procedure is used as the high-frequency cut-off when applying a five pole Butterworth filter to a trace. Each trace is independently low-pass filtered with a high-frequency cut-off determined by the frequency of the observed pulse and the noise level of the trace. When this low-pass filtering is performed, it effectively removes the bias in the mean differential attenuation values as shown in Figs 10(a) and (b). This method is termed instantaneous-frequency matching with filtering, or IFM/F.

In the next example, the same 50 noisy seismic sections are used to test the spectral-ratio method. The spectral-ratio method with a fixed bandwidth of 10–60 Hz is used in Fig. 11, and illustrates why a variable bandwidth is needed when using spectral ratios. A significant bias in the estimated mean attenuation values is shown in Fig. 11(b). While a large bandwidth is desirable for spectral ratios when the signal-to-noise ratio is high, with increasing propagation distance the higher frequencies of the Gabor wavelet are attenuated to the noise level. This causes a decrease in the slope of the least-squares line fit. As shown in Fig. 11, an improper selection of bandwidth for spectral ratios has a much more dramatic effect on the calculated attenuation values than it did when using instantaneous-frequency matching. By using a variable bandwidth for the spectral ratios, or SR/VB, based on the frequency where the pulse spectrum is reduced to the noise level, this bias can be removed, as shown in Fig. 12.

The variable cut-off filtering for instantaneous-frequency matching (IFM/F) and the variable bandwidth for the spectral

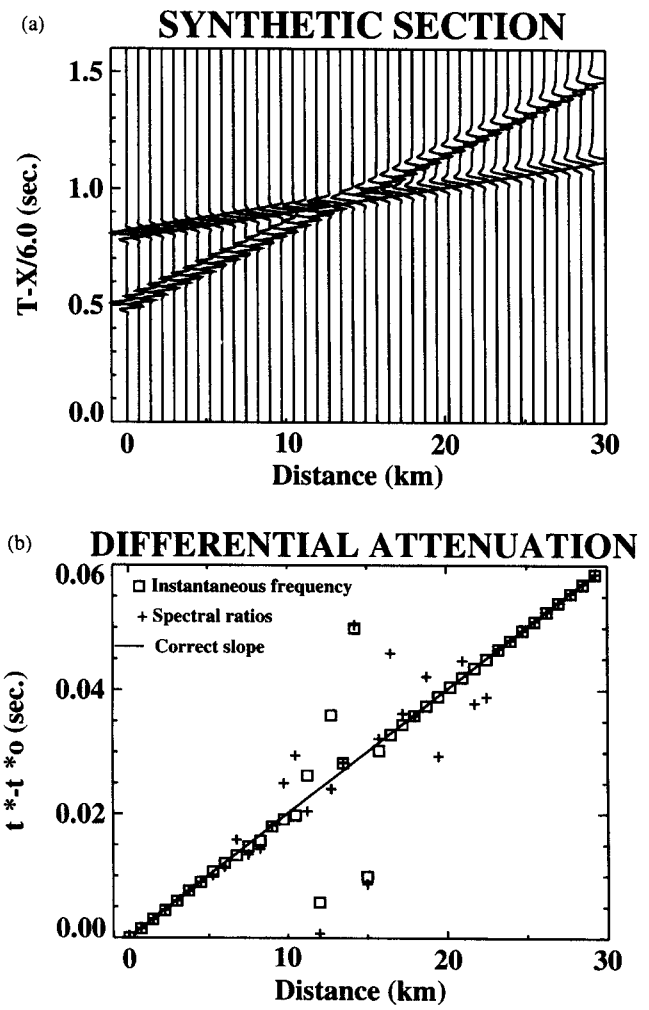

Figure 13. Synthetic section example with interfering arrivals. (a) Synthetic section with one wavelet propagating with a velocity of 5.0 km s^{-1} in a medium with a Q of 100 and the other wavelet propagating at 5.2 km s^{-1}. (b) The resulting differential attenuation values using both instantaneous frequency and spectral ratios.

ratios (SR/VB) are necessary to remove biasing of the calculated attenuation values due to random noise. The standard deviations of the calculated differential attenuation values determined using instantaneous frequencies, however, are typically less than those from spectral ratios (Figs 10b and 12b). Thus instantaneous-frequency matching results in attenuation values with less scatter than those from the spectral ratios in the presence of random noise.

The final synthetic example, shown in Fig. 13, examines the effect of interference from secondary arrivals on the differential attenuation values. A Gabor wavelet propagating with a velocity of 5.0 km s^{-1} in a medium with $Q = 100$ is used. In addition, a second Gabor wavelet propagating with a velocity of 5.2 km s^{-1} is included. The calculated differential attenuation values are correct using both the IFM/F and SR/VB methods for distances less than 7.0 km or greater than 24.0 km. Between 7.0 km and 24.0 km, the spectral ratio estimates start to diverge from the correct values. This is due to the windowing of the P wave that is required for the spectral-ratio method. The secondary arrivals result in holes in the spectral ratios, which in turn can bias the attenuation estimates. Instantaneous-frequency matching utilizes a more isolated estimate of the attributes of the first arrival then does the spectral-ratio method, and is less affected by secondary arrivals. Where the interfering pulses significantly overlap, between 11.0 and 17.0 km, neither method can be used to extract the correct attenuation value. For this case, a check must be provided such that, if the signal envelope does not decrease sufficiently after the first-arrival envelope peak, the trace is not used.

COMPARISON OF THE METHODS USING 1986 OUACHITA PASSCAL REFRACTION DATA

The instantaneous-frequency matching and spectral-ratio methods are applied to observed refraction data from the 1986 PASSCAL Ouachita experiment. The Ouachita experiment consists of a 200 km seismic profile into which 29 shots were fired. Seismic group recorders with a spacing of 250 m were used to record the data (Keller *et al.* 1989; Lutter & Nowack 1990). The multiple-shot layout of the experiment, along with the dense receiver coverage, makes the Ouachita data set well suited for the testing of attenuation algorithms. Shot gathers from the northern half of the seismic experiment were used, rather than those from the southern half, which have higher noise levels. A typical shot gather from the northern segment of the experiment, shot gather 2.0, is shown in Fig. 14. In this figure, the shot is located at 0 km and every fifth trace is plotted. Pulse broadening of the first-arrival P wave can be observed as the distance from the shot is increased.

Using Ouachita shot gathers 1.3 and 2.0 as examples, the derived differential attenuation values using both filtered, instantaneous-frequency matching (IFM/F) and variable-bandwidth spectral ratios (SR/VB) are shown in Figs 15(a) and 16(a). The differential attenuation values obtained from IFM/F are consistent with those derived using SR/VB. Also, the attenuation values calculated from IFM/F have less scatter than those from SR/VB. This is to be expected since the synthetic tests showed the spectral-ratio method to be more dramatically affected by random noise and secondary arrivals than the instantaneous-frequency matching method.

Once the differential attenuation values for all the traces are calculated, the values derived from IFM/F are interpolated onto a regular-interval grid and smoothed, as shown in Figs 15(b) and 16(b). This is done by applying a splines-under-tension algorithm (Cline 1974) with a tension of 3.0 to interpolate the differential attenuation value onto a 0.2 km grid. A 19 point boxcar averaging filter is then used to smooth the observed values. Finally, the values are re-interpolated onto a 1.0 km interval grid. This interpolation and smoothing process results in a regularly spaced grid of points and averages some of the scatter caused by random noise and secondary arrivals. The smoothing, though, comes at the expense of losing some of the details of the differential attenuation profile.

The differential attenuation profiles for the other Ouachita shot gathers are similar in appearance. They have sharply increasing differential attenuation values near the shot and a more gradual roll-off to a lower slope as the distance from the shot increases. This is due to near-surface rocks that result in a high level of attenuation and a decrease in attenuation with depth. As an example, for shot gather 1.3, differential t^* values between the reference pulse, located at 1.87 km, and receivers located at distances of 15.87 and 28.87 km are 0.0376 and

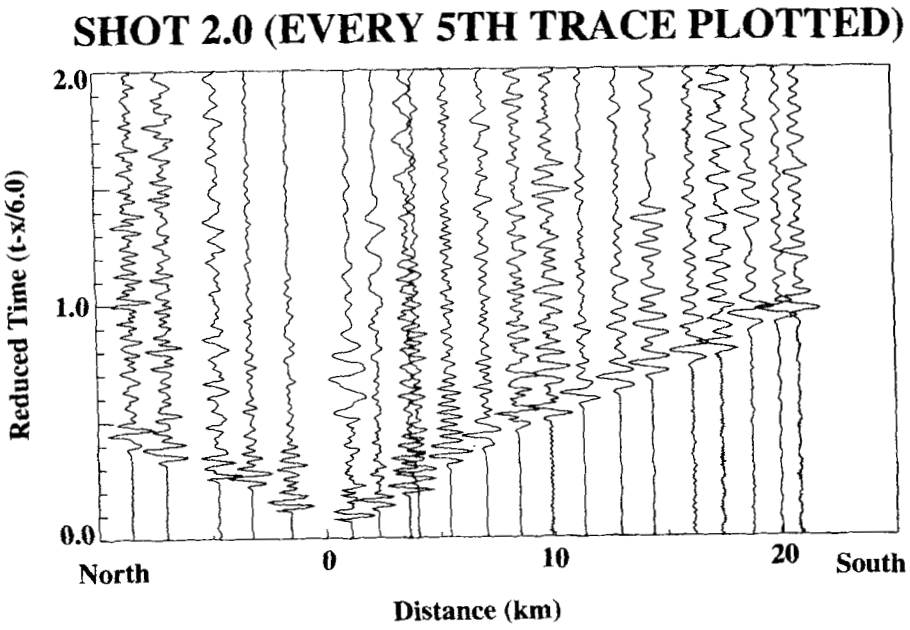

Figure 14. Typical shot gather for the northern part of the 1986 PASSCAL Ouachita experiment (shot gather 2.0).

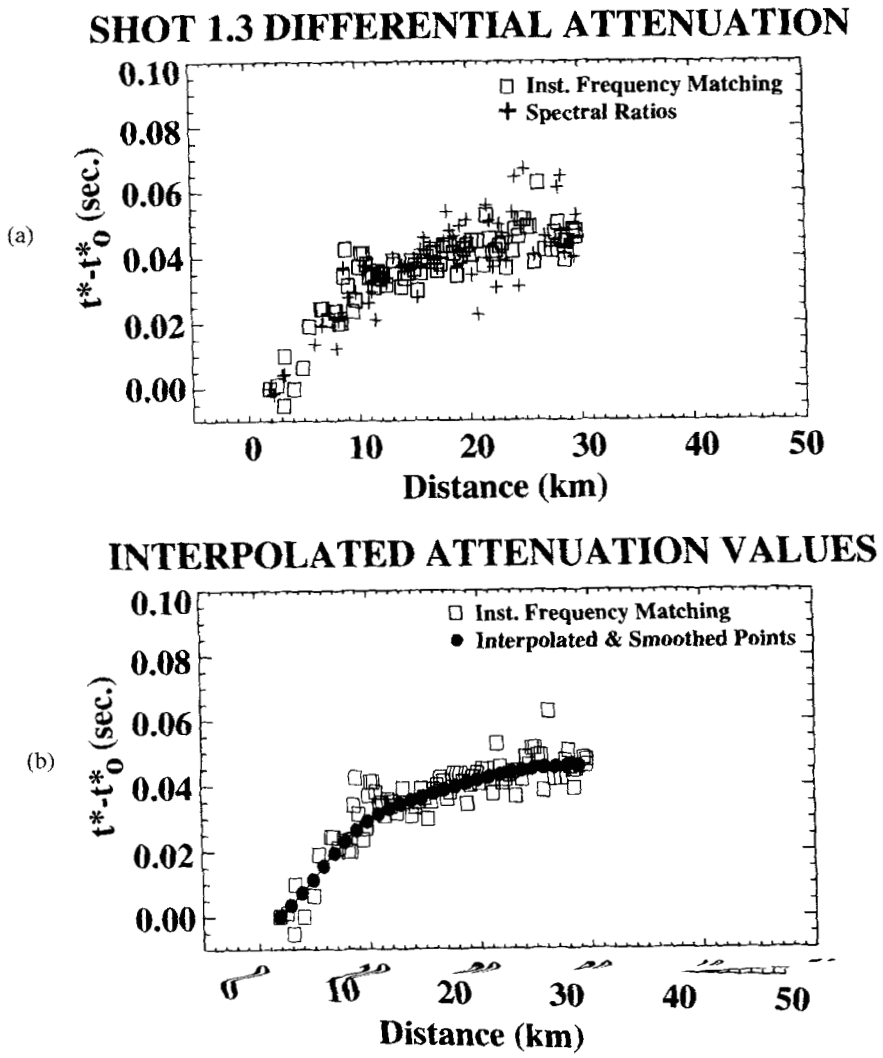

Figure 15. (a) Differential attenuation values obtained using the filtered instantaneous-frequency matching (IFM/F) and spectral-ratio (SR/VB) methods on Ouachita shot gather 1.3. (b) The interpolated and smoothed differential attenuation values obtained using IFM/F.

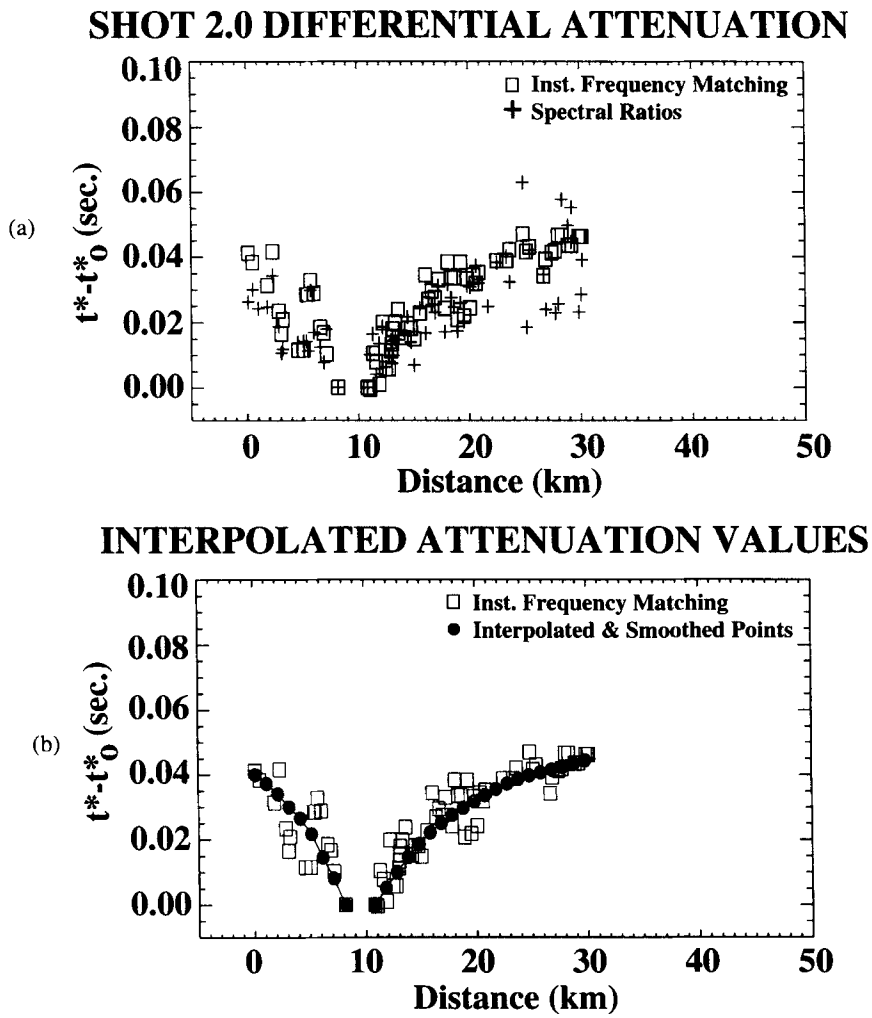

Figure 16. (a) Differential attenuation values obtained using the filtered intantaneous-frequency matching (IFM/F) and spectral-ratio (SR/VB) methods on Ouachita shot gather 2.0. (b) The interpolated and smoothed differential attenuation values obtained using IFM/F.

0.0459 s, respectively. Using eq. (12) with the reference arrival time of 0.377 s and arrival times of 3.272 and 5.832 s for the two receivers, the average Q values are 77 for the receiver at 15.87 km and 119 for the receiver at 28.87 km. A simultaneous inversion using traveltimes and differential attenuation to obtain subsurface velocity and Q structure will be included in a subsequent paper.

CONCLUSIONS

Differential attenuation values were derived using filtered instantaneous-frequency matching (IFM/F) and variable-bandwidth spectral ratios (SR/VB). The methods are consistent with one another, with IFM/F less sensitive to noise than SR/VB. For spectral ratios, there is a trade-off when selecting a window length between good stability with a large window length but many spectral holes, and a short window length that eliminates spectral holes but makes the calculated attenuation values highly variable. The use of a variable window length, based on the arrival time to peak envelope amplitude, provides a good compromise and gives stable results. For the case of instantaneous-frequency matching, only the windowing of a reference pulse is required.

When estimating attenuation, a spectral bandwidth must also be selected. A reasonable choice is to select a bandwidth that includes as much of the usable spectrum as possible. This is accomplished by using a variable bandwidth that is based on the background noise level of the trace. A variable bandwidth provides unbiased and stable results for the spectral-ratio attenuation estimates. When using instantaneous-frequency matching, noise in the seismic trace can increase the instantaneous-frequency estimates, and thus lower the differential attenuation values. This bias can be removed by using a variable-bandwidth filter that has a cut-off frequency determined by the noise level of the trace.

Using both synthetic and observed data, instantaneous-frequency matching with filtering (IFM/F) provides attenuation estimates consistent with those from spectral ratios (SR/VB), while having less scatter. The attenuation results from instantaneous-frequency matching were found to be less affected by random noise and second arrivals than those from spectral ratios.

ACKNOWLEDGMENTS

This work was supported by the NSF Grant No. EAR-9018217.

REFERENCES

Aki, K. & Richards, P., 1980. *Quantitative Seismology, Theory and Methods,* Freeman and Co., New York.

Badri, M. & Mooney, H.M., 1987. Q measurements from compressional seismic waves in unconsolidated sediments, *Geophysics,* **52,** 772–784.

Barnes, A.E., 1991. Instantaneous frequency and amplitude at the envelope peak of a constant-phase wavelet, *Geophysics,* **56,** 1058–1060.

Barnes, A.E., 1993. Instantaneous spectral bandwidth and dominant frequency with applications to seismic reflection data, *Geophysics,* **58,** 419–428.

Bath, M., 1974. *Spectral Analysis In Geophysics,* Elsevier, Amsterdam.

Blair, D.P. & Spaths, A.T., 1984. Seismic source influence in pulse attenuation studies, *J. Geophys. Res.,* **89,** 9253–9258.

Braile, L., 1977. *The Earth's Crust,* AGU Monograph Series, no. 20, Am. Geophys. Un., Washington, DC.

Brzostowski, M.A. & McMechan, G.A., 1992. 3-D tomographic imaging of near-surface seismic velocity and attenuation, *Geophysics,* **57,** 396–403.

Carpenter, P.J. & Sanford, A.R., 1985. Apparent Q for upper crustal rocks of the central rio grande rift, *J. Geophys. Res.,* **90,** 8661–8674.

Červený, V., Molotkov, I.A. & Pšenčík, I., 1977. *Ray Methods in Seismology,* Karlova Universita, Prague.

Cline, A., 1974. Scalar- and planar-valued curve fitting using splines under tension, *Comm. ACM.,* **17,** 218–223.

Gabor, D., 1946. Theory of communication, *Proc. Inst. Elec. Eng.,* **93,** 429–457.

Gladwin, M.T. & Stacey, F.D., 1974. Anelastic degradation of acoustic pulses in rock, *Phys. Earth planet. Int.,* **8,** 332–336.

Ingram, J.D., Morris, C.F., MacKnight, E.E. & Parks, T.W., 1985. Direct determination of S-wave velocities from acoustic waveform logs, *Geophysics,* **50,** 1746–1755.

Jannsen, D., Voss, J. & Theilen, F., 1985. Comparison of methods to determine Q in shallow marine sediments from vertical reflection seismograms, *Geophys. Prospect.,* **33,** 479–497.

Keller, G.R., Braile, L.W., McMechon, G.A., Thomas, W.A., Harder, S.H., Chang, W.F. & Jardine, W.G., 1989. The Paleozoic continent–ocean transition in the Ouachita mountains imaged from PASSCAL wide angle seismic reflection–refraction data, *Geology,* **17,** 119–122.

Lutter, W.J. & Nowack, R.L., 1990. Inversion for crustal structure using reflections from the PASSCAL Ouachita experiment, *J. Geophys. Res.,* **95,** 4633–4646.

Press, W.H., Teukolsky, S.A., Vetterling, W.T. & Flannery, B.P., 1992. *Numerical Recipes in Fortran,* 2nd edn, Cambridge Univ. Press, New York.

Saha, J.G., 1987. Relationship between Fourier and instantaneous frequency, 57th Ann. Int. Mtg, *Soc. Expl. Geophys. Expanded Abstracts,* 591–594.

Sams, M. & Goldberg, D., 1990. The validity of Q estimates from borehole data using spectral ratios, *Geophysics,* **55,** 97–101.

Taner, M.T., Koehler, F. & Sheriff, R.E., 1979. Complex seismic trace analysis, *Geophysics,* **44,** 1041–1063.

Tarif, P. & Bourbie, T., 1987. Experimental comparisons between spectral ratio and rise time techniques for attenuation measurement, *Geophys. Prospect.,* **35,** 668–680.

Tonn, R., 1989. Comparison of seven methods for the computation of Q, *Phys. Earth planet. Int.,* **55,** 259–268.

Tonn, R., 1991. The determination of the seismic quality factor Q from VSP data: a comparison of different computational methods, *Geophys. Prospect.,* **39,** 1–27.

White, R.E., 1992. The accuracy of estimating Q from seismic data, *Geophysics,* **57,** 1508–1511.

Wright, C. & Hoy, D., 1981. A note on pulse broadening and anelastic attenuation in near-surface rocks, *Phys. Earth planet. Int.,* **25,** P1–P8.